Aerospace Science and Technology 91 (2019) 656–668

Contents lists available at ScienceDirect

Aerospace Science and Technology

www.elsevier.com/locate/aescte

Comprehensive assessment of newly-developed slip-jump boundary conditions in high-speed rarefied gas flow simulations

Nam T.P. Le [a,b], Ehsan Roohi [c,*], Thoai N. Tran [d]

[a] Divison of Computational Mathematics and Engineering, Institute for Computational Science, Ton Duc Thang University, Ho Chi Minh City, Viet Nam
[b] Faculty of Civil Engineering, Ton Duc Thang University, Ho Chi Minh City, Viet Nam
[c] High Performance Computing (HPC) Laboratory, Department of Mechanical Engineering, Faculty of Engineering, Ferdowsi University of Mashhad, P.O. Box 91775-1111, Mashhad, Iran
[d] Faculty of Mechanical Engineering, Industrial University of Ho Chi Minh City, Viet Nam

ARTICLE INFO

Article history:
Received 18 January 2019
Received in revised form 23 May 2019
Accepted 3 July 2019
Available online 9 July 2019

Keywords:
Rarefied gas flows
Slip-jump boundary conditions
Aoki et al. conditions
Slip velocity
Surface gas temperature

ABSTRACT

In this paper we numerically evaluate the recently developed Aoki et al. slip and jump conditions in high-speed rarefied gas flows for the first time. These slip and jump conditions are developed to be employed with the Navier–Stokes–Fourier equations. They were derived based on the Boltzmann equation with the first order Chapman–Enskog solution, and the analysis of the Knudsen layer. Four aerodynamic configurations are selected for a comprehensive evaluation of these conditions such as sharp-leading-edge flat plate, vertical plate, wedge and circular cylinder in cross-flow with the Knudsen number varying from 0.004 to 0.07, and argon as the working gas. The simulation results using the Aoki et al. boundary conditions show suitable agreement with the DSMC data for slip velocity and surface gas temperature. The accuracy of these boundary conditions is superior to the conventional Maxwell, Smoluchowski and Le boundary conditions.

1. Introduction

Rarefied gas flow generally has four distinct regimes. They are characterized according to their Knudsen number, Kn, that it is defined as the ratio of gas mean free path, i.e., the average distance a molecule moves between successive intermolecular collisions, to a characteristic length of the vehicle body. The continuum regime corresponds to very small Kn number, $Kn \leq 0.001$. The slip regime with the temperature jump and slip velocity conditions at the surface is indicated by the range $0.001 \leq Kn \leq 0.1$. When the gas flows become more and more rarefied then they are characterized as the transition and free molecular regimes, respectively. The transition-continuum regime corresponds to $0.1 \leq Kn \leq 1$, and the free molecular regime to $Kn \geq 1$. Two typical methods have been used to solve the rarefied gas flows such as Direct Simulation Monte-Carlo (DSMC) and Computational Fluid Dynamics (CFD). The DSMC method has successfully simulated the rarefied gas flows for four regimes aforementioned, but its computational effort is quite expensive at small Knudsen number conditions. The CFD method that solves the Navier–Stokes–Fourier (N–S–F) equations accompanied with appropriate slip and jump boundary conditions may successfully simulate the rarefied gas flows in the slip regime and even beyond. The slip and jump conditions play an essential role in the accurate prediction of the surface quantities. During the last decades, several slip and jump boundary conditions were developed based on the kinetic theory of gases, the Langmuir isotherm adsorption, and combination of the Langmuir isotherm adsorption and kinetic theory of gases in [1–9] to work with the N–S–F equations to simulate the rarefied gas flows. However, they have not yet predicted well the surface quantities in rarefied gas simulations.

The rarefied gas flow cannot be described by the ordinary macroscopic equations. In [10,11] the slip and jump boundary conditions have been recently derived from the Boltzmann equations on the basis of the first-order Chapman–Enskog solution of the Boltzmann equation, and the analysis of the Knudsen layer adjacent to the boundary. These conditions were developed for large density and temperature variation to employ with the compressible N–S–F equations. They were derived for the rarefied gas flows applied to monatomic gas in [10], and polyatomic gas in [11]. They have been used and evaluated for the numerical analysis of the Taylor-vortex flow in [12]. In this paper, we only focus on the revisit and assessment of the slip and jump boundary conditions for the monatomic gas in [10].

As for the Aoki et al. slip and jump conditions derived for polyatomic gases in [11], we need to determine the term related to the

* Corresponding author.
E-mail addresses: letuanphuongnam@tdtu.edu.vn (N.T.P. Le), e.roohi@ferdowsi.um.ac.ir (E. Roohi), tranngocthoai@iuh.edu.vn (T.N. Tran).

https://doi.org/10.1016/j.ast.2019.07.005
1270-9638/

Table 1
List of all CFD cases.

Cases	Kn	Mach number, Ma	Gas
Sharp-leading-edge flat plate	0.0042	4	Argon
Vertical flat plate	0.07	3	Argon
Circular cylinder in cross-flow	0.01; 0.05	10	Argon
Sharp-leading edge wedge	0.05	10	Argon

collision frequency of the gas molecules that they cannot be calculated in CFD. The surface quantities such as the pressure, temperature and slip velocity using the Aoki et al. slip and jump conditions are compared with those using the conventional Maxwell slip condition, the Smoluchowski jump condition, and DSMC data. Recently, the temperature jump boundary conditions were developed based on the kinetic theory of gases considering the viscous heat generation in [13,14]. These jump conditions improved the prediction of the surface gas temperatures in comparing with those using the classical Smoluchowski jump condition, and gave good agreement with the DSMC data. So, the surface gas temperatures using the Aoki et al. jump condition are also compared with those using the temperature jump condition considering the viscous heat generation [14]. Four aerodynamic configurations including the sharp and blunt bodies are selected to assess the Aoki et al. slip and jump conditions in predicting the surface quantities, and they are presented in Table 1.

2. Slip and jump boundary conditions in CFD and slip quantities in DSMC

The temperature and velocity of the rarefied gas at a surface are not equal to the wall temperature and the wall velocity, respectively. This results in the slip and jump boundary conditions need to be derived in simulations of the rarefied gas flows. In this section, we revisit the classical slip and jump conditions in CFD. The conventional Maxwell slip velocity condition, including the effect of the curvature and thermal creep, can be expressed as [1]:

$$\mathbf{u}+\left(\frac{2-\sigma_{\mathrm{u}}}{\sigma_{\mathrm{u}}}\right)\lambda\nabla_{\mathbf{n}}(\mathbf{S}\cdot\mathbf{u}) = \mathbf{u}_{\mathrm{w}}-\left(\frac{2-\sigma_{\mathrm{u}}}{\sigma_{\mathrm{u}}}\right)\frac{\lambda}{\mu}\mathbf{S}\cdot(\mathbf{n}\cdot\mathbf{\Pi}_{\mathrm{mc}})-\frac{3}{4}\frac{\mu}{\rho}\frac{\mathbf{S}\cdot\nabla T}{T}, \tag{1}$$

where tensor $\mathbf{S}=\mathbf{I}\text{-}\mathbf{nn}$, where $\mathbf{n}$ is the unit normal vector defined as positive in the direction pointing out of the flow domain, removes normal components of any non-scalar field, e.g., velocity, so that slip only occurs in the direction tangential to the surface; the symbol '·' is the inner product; λ is the mean free path; μ is the viscosity; ρ is the density; T is the temperature; $\mathbf{u}$ is the slip velocity; and $\mathbf{u}_{\mathrm{w}}$ is the wall velocity. The tangential momentum accommodation coefficient determines the proportion of molecules reflected from the surface specularly (equal to $1-\sigma_{\mathrm{u}}$) or diffusely (equal to σ_{u}), and $0\le\sigma_{\mathrm{u}}\le 1$. Tensor $\Pi_{\mathrm{mc}}=\mu((\nabla\mathbf{u})^{\mathrm{T}}-\frac{2}{3}\mathbf{I}\,\mathrm{tr}(\nabla\mathbf{u}))$; superscript T stands the transpose; and tr is the trace. The right-hand side of equation (1) contains 3 terms associated with (in order): the wall velocity, the so-called curvature effect, and thermal creep. The Maxwellian mean free path is defined as follows [15]:

$$\lambda=\frac{\mu}{\rho}\sqrt{\frac{\pi}{2RT}}, \tag{2}$$

where R is the specific gas constant. The viscosity is calculated by the Sutherland law,

$$\mu=A_{\mathrm{S}}\frac{T^{1.5}}{T+T_{\mathrm{S}}}, \tag{3}$$

where the coefficients $A_{\mathrm{S}}=1.93\times10^{-6}$ Pa s K$^{-1/2}$ and $T_{\mathrm{S}}=142$ K for argon [3].

In rarefied gas flows, the gas temperature at a surface is not equal to the wall temperature, and this difference is called the temperature jump. The classical Smoluchowski temperature jump condition is derived by the heat flux normal to the surface, and can be written [2]:

$$T+\frac{2\sigma_T}{\sigma_T}\frac{2\gamma}{(\gamma+1)\mathrm{Pr}}\lambda\nabla_{\mathbf{n}}T=T_{\mathrm{w}}, \tag{4}$$

where γ is the specific heat ratio; Pr is the Prandtl number; T_{w} is the wall temperature, and σ_T is the thermal accommodation coefficient that varies from 0 to 1. Perfect energy exchange between the gas and the solid surface corresponds to $\sigma_T=1$, and no energy exchange to $\sigma_T=0$.

Recently, the temperature jump conditions were derived by considering viscous heat generation in heat flux at the surface [13,14]. The viscous heat generation was first introduced by Maslen in [16]. The modified Patterson jump condition was developed in [14], *so-called Le jump condition* in the present work. It predicted better temperatures than the new type of the Smoluchowski jump condition [13] in high-speed rarefied gas flow simulations. Therefore, the Le jump condition is adopted for simulations, and is expressed as follows [14]

$$T+\frac{1}{2}\left(\frac{2-\sigma_T}{\sigma_T}\right)\frac{\gamma}{\gamma-1}\frac{T_{\mathrm{w}}}{T}\frac{\lambda}{\mathrm{Pr}}\nabla_{\mathbf{n}}T = T_{\mathrm{w}}-\frac{1}{2}\left(\frac{2-\sigma_T}{\sigma_T}\right)\frac{1}{c_v(\gamma-1)}\frac{T_{\mathrm{w}}}{T}\frac{\lambda}{\mu}\big(\mathbf{S}\cdot(\mathbf{n}\cdot\mathbf{\Pi})\cdot\mathbf{u}\big), \tag{5}$$

where c_v is the specific heat of the gas at the constant volume; and $\mathbf{\Pi}$ is the stress tensor. The second term in the right-hand side of equation (5) presents the viscous heat generation part.

Alternative slip and jump conditions were recently developed for rarefied gas flow based on the Boltzmann equations with the first-order Chapman–Enskog solution of the Boltzmann equations. Moreover, the analysis of the Knudsen layer adjacent to the boundary, and kinetic corrections of the macroscopic quantities inside the Knudsen layer were also involved in the derivation of the slip and jump conditions. They were derived for monatomic and polyatomic gases in [10,11] with the accommodation coefficients of unity, the *so-called Aoki et al. slip and jump conditions* in the present work. They are presented in equations (6) and (7) respectively, as [10]

$$\mathbf{u}+\sqrt{\frac{2}{R}}a_{\mathrm{vI}}\frac{\mu_{\mathrm{w}}}{\rho\sqrt{T_{\mathrm{w}}}}\nabla_{\mathbf{n}}(\mathbf{S}\cdot\mathbf{u})=\mathbf{u}_{\mathrm{w}}+\frac{4}{5R}a_{\mathrm{TI}}\frac{k_{\mathrm{w}}}{\rho T_{\mathrm{w}}}(\mathbf{S}\cdot\nabla T), \tag{6}$$

and

$$T+\frac{2}{5R}\sqrt{\frac{2}{R}}a_{\mathrm{TII}}\frac{k_{\mathrm{w}}}{\rho\sqrt{T_{\mathrm{w}}}}\nabla_{\mathbf{n}}T=T_{\mathrm{w}}+\frac{1}{R}a_{\mathrm{vII}}\frac{\mu_{\mathrm{w}}}{\rho}\big((\nabla\mathbf{u}\cdot\mathbf{n})\cdot\mathbf{n}\big), \tag{7}$$

where k_{w} and μ_{w} are the thermal conductivity and viscosity at the wall temperature, respectively. For the hard-sphere molecule, the coefficients (a_{vI}, a_{vII}, a_{TI}, a_{TII}) in equations (6) and (7) have the values as follows [10] $a_{\mathrm{vI}}=0.98733$; $a_{\mathrm{vII}}=0.36185$; $a_{\mathrm{TI}}=0.33628$; and $a_{\mathrm{TII}}=1.24859$.

Thermal conductivity k_{w} and viscosity μ_{w} are calculated as [10],

$$\mu_{\mathrm{w}}=0.17913618\frac{m\sqrt{R}}{d^2}\sqrt{T_{\mathrm{w}}}, \tag{8}$$

and

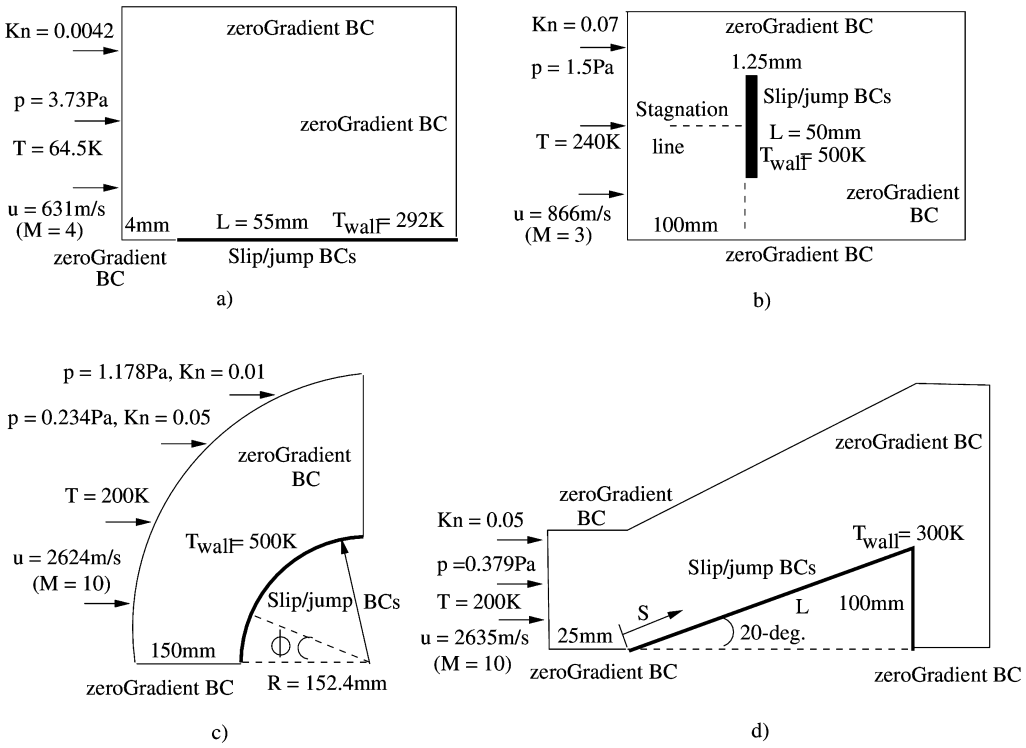

Fig. 1. The geometries, freestream conditions, and CFD numerical setups of cases a) sharp-leading-edge flat plate, b) vertical flat plate, c) circular cylinder, and d) sharp-leading-edge wedge.

$$k_w = 0.67783290\frac{mR\sqrt{R}}{d^2}\sqrt{T_w}, \tag{9}$$

where m is mass of a molecule; and d is diameter of molecule.

It is noticed that the classical Smoluchowski jump condition (Eq. (4)) is independent of the velocity of gas flow near the surface, while the Le and Aoki et al. jump conditions are dependent the velocity and gradient of the velocity of gas flow near the surface. All slip and jump conditions aforementioned (Equations (1), (4), (5), (6) and (7)) are implemented in OpenFOAM [17] to work with the N–S–F equations that are numerically solved using a finite volume discretization and high-resolution central schemes in the solver *rhoCentralFoam* to simulate high-speed viscous flows. A calorically perfect gas for which $p = \rho RT$ is assumed in this solver. The implemented approach of the slip and jump conditions in OpenFOAM was described in [3].

Finally, the slip velocity and surface gas translational temperature in DSMC are treated in the post-process [18], and they are calculated with the accommodation coefficients of unity as follows [19]:

$$\mathbf{u} = \frac{\sum((m/u_n)u_p)}{\sum(m/u_n)} - \mathbf{u}_w, \tag{10}$$

$$T = \frac{\sum((m/u_n)\|\mathbf{u}^2\|) - \sum(m/u_n)\mathbf{u}^2}{3k_B\sum(1/u_n)} - T_w, \tag{11}$$

where k_B is the Boltzmann constant; and $\|\mathbf{u}\|$ is the velocity magnitude. The velocity normal to the surface, u_n, and the velocity parallel to the surface, u_p, in equations (10) and (11) are taken prior to and after the collision with the surface. The summations include pre-collision and post-collision molecules. Equation (11) points out that the surface gas translational temperature in DSMC is addressed as a function of velocity.

Table 2
Mesh cell sizes of all CFD cases.

Cases	Δx (mm)	Δy (mm)
Flat plate	0.1	0.15
Vertical plate	0.25	0.25
Cylinder	0.15	0.3
Wedge	0.25	0.25

3. Numerical setup

In OpenFOAM the model is often built in three-dimensional. Our CFD and DSMC two-dimensional simulations are carried out by applying the condition “empty” to patches that do not constitute the solution direction. The geometries, freestream conditions, and computational domains of all cases are presented in Figs. 1a, 1b, 1c and 1d. The freestream conditions of (p, T, $\mathbf{u}$) are applied to the inlet boundary, and are maintained through the computational process. The zeroGradient condition is applied to other boundaries so that fluid is allowed to leave the computational domain. This condition specifies that the normal gradients of the flow variables (p, T, $\mathbf{u}$) vanish at those boundaries. The simulations of the circular cylinder in cross-flow are carried out for the cylinder forebody, and their freestream conditions are adopted in [20].

The hexahedral structured mesh is selected for all cases. The computational mesh is constructed to wrap around the oblique and bow shocks. The mesh independence is conducted to obtain the final mesh for all cases. The smallest cell sizes near the surfaces of all CFD cases are presented in Table 2. The rectangular mesh is used for the sharp-leading-edge flat plate and vertical plate cases. The mesh of the flat plate case is quite simple, and only that of the vertical plate case is presented here. Typical meshes of the vertical plate, cylinder and wedge cases are found in Figs. 2a, 2b and 2c, respectively.

Various slip and jump boundary conditions are applied to the surfaces. The Knudsen-layer correction [10] was not implemented in our CFD simulations. We use three different slip and jump mod-

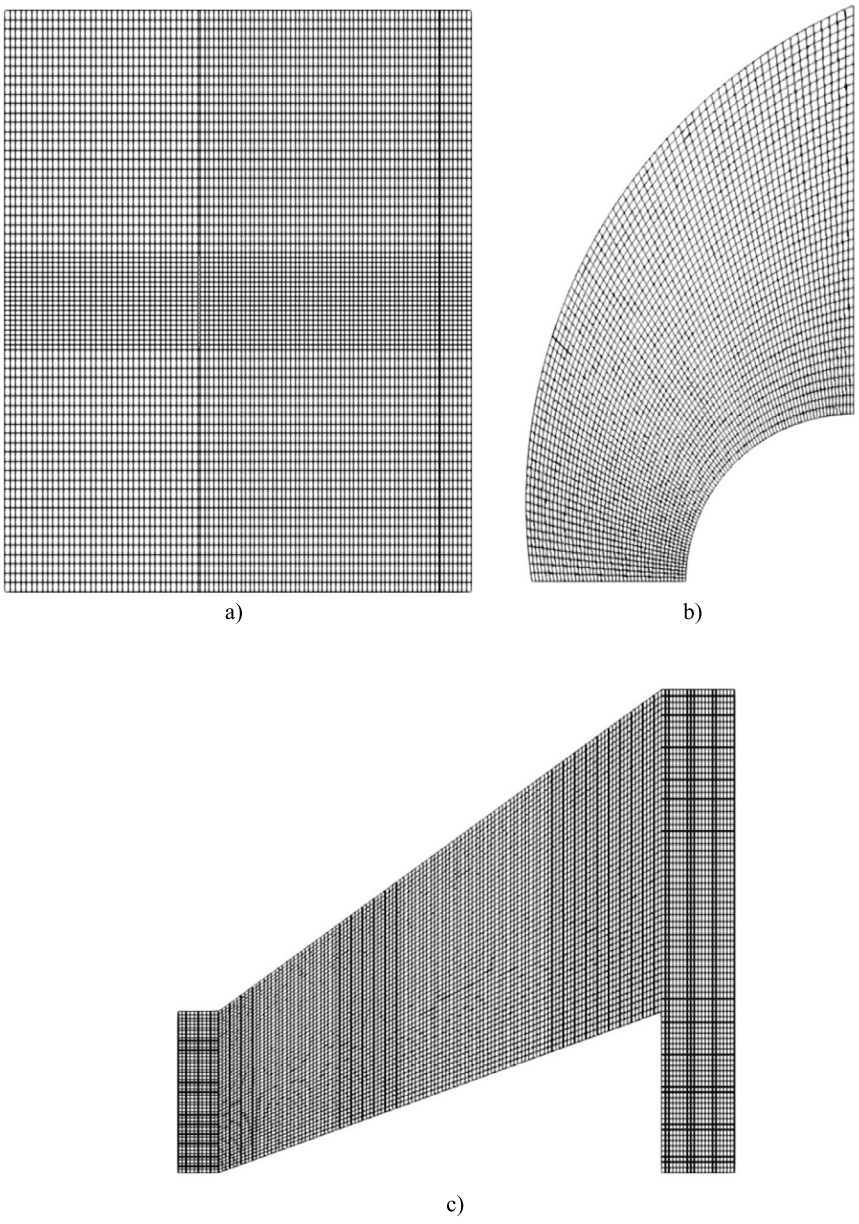

Fig. 2. Typical structured meshes of a) the vertical plate, b) circular cylinder (Kn = 0.01) and c) wedge cases (every fifth line presented).

els for the CFD simulations in the present work as follows: 1) the classical Maxwell-Smoluchowski boundary conditions (BCs), 2) the Aoki et al. slip and the Le jump BCs, and 3) the Aoki et al. slip and jump BCs. Argon gas is used for all CFD and DSMC simulations of cases. The solver dsmcFoam in OpenFOAM is used to run the DSMC simulations. The hard-sphere molecular model is adopted for all DSMC cases because the coefficients (a_{vI}, a_{vII}, a_{TI}, a_{TII}) of the Aoki et al. slip and jump conditions are computed for the hard-sphere molecule. A structured mesh is also used in the DSMC simulations. The cell size is determined by the freestream mean free path, λ_∞, that it is calculated by the freestream (pre-shock) gas flow conditions. A cell size of approximately $\lambda_\infty/3$ is used in all DSMC simulations. The tangential and thermal accommodation coefficients of unity are used for all DSMC and CFD simulations.

4. Simulation results

The simulation results such as the surface pressure, surface gas temperature, slip velocity are plotted against the cylinder angle, ϕ, for the cylinder cases, and the normalized distances, where distances are normalized by their lengths, for the flat plate, vertical plate and wedge cases. Moreover, the temperature and velocity magnitude contours of the DSMC solutions and CFD simulations using the Aoki et al. conditions, are also presented in this section for all cases.

4.1. Sharp-leading-edge flat plate case, Kn = 0.0042

The simulation results of the sharp-leading-edge flat plate case are presented in Figs. 3, 4, 5, 6, 7, and 8. They are plotted against x/L, where x runs from the tip to the tail of the flat plate, and L is the length of the flat plate. Fig. 3 presents the distribution of the surface gas pressure over the flat plate. At the leading edge, surface gas pressures of all CFD runs obtain the peak values of 1) 26.5 Pa for the Maxwell–Smoluchowski conditions, 2) 31.06 Pa for the Aoki et al. and Le conditions, 3) 28.1 Pa for the Aoki et al. conditions, and 4) 13.51 Pa for the DSMC data. Past the peak location, all CFD and DSMC simulation results gradually decrease

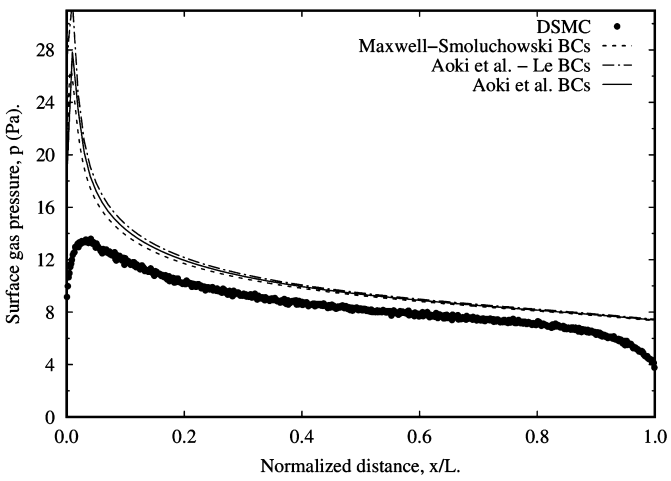

Fig. 3. Distribution of surface gas pressure over the flat plate.

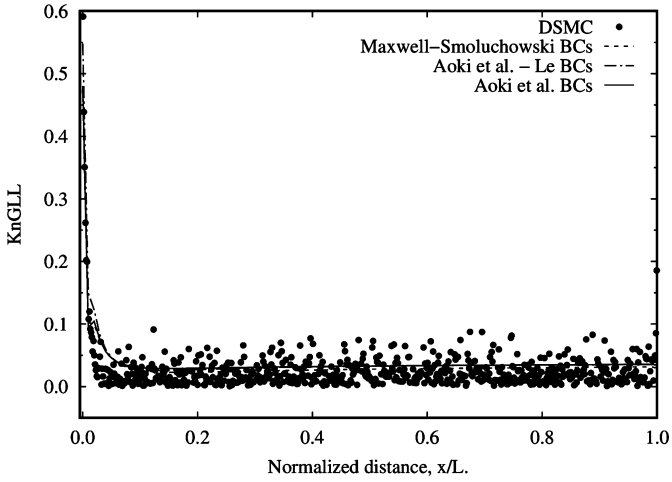

Fig. 4. Distribution of KnGLL over the flat plate.

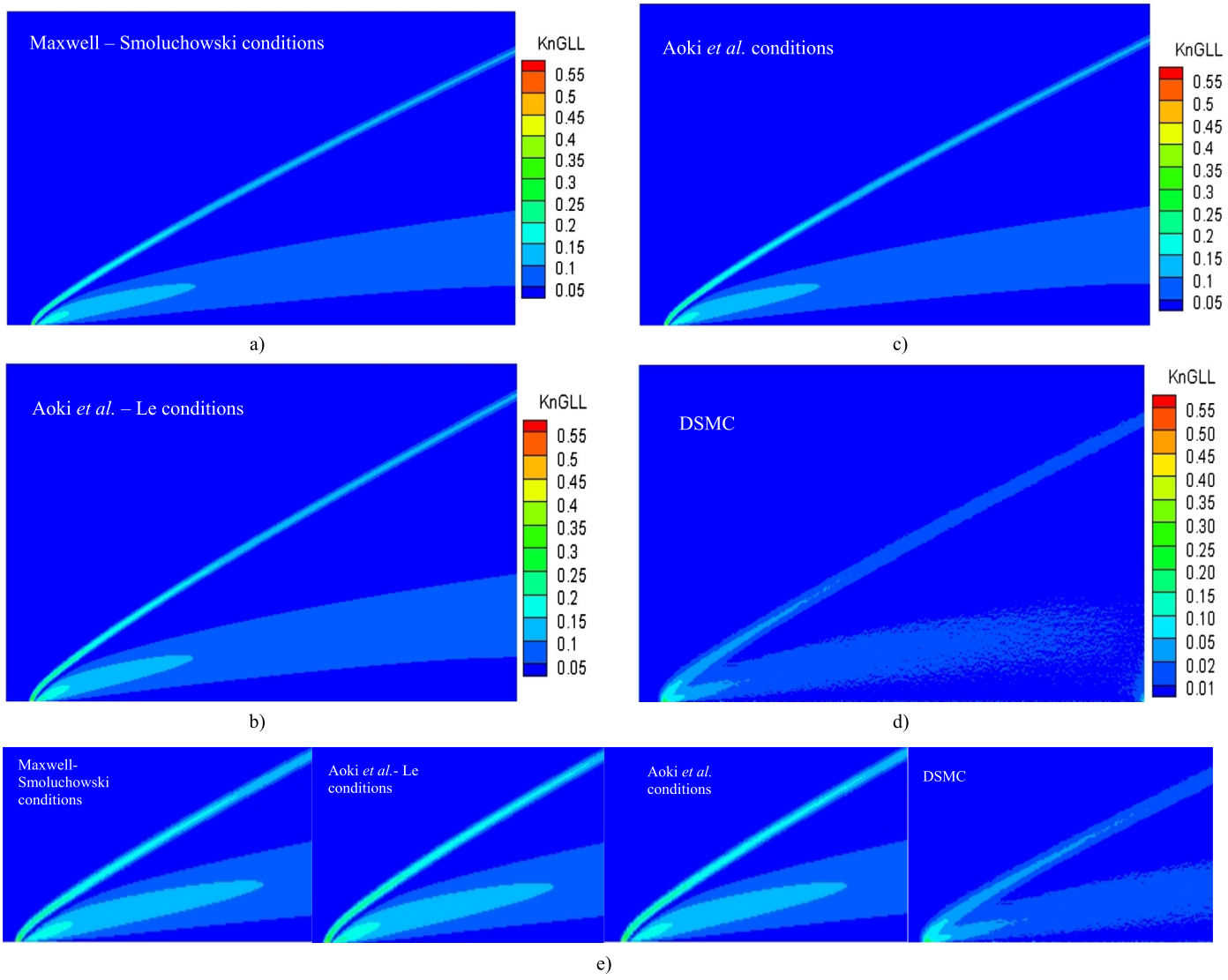

Fig. 5. The Kn_{GLL} contours of CFD and DSMC simulations, a) Maxwell–Smoluchowski condition, b) Aoki et al. – Le conditions, c) Aoki et al. conditions, d) DSMC, and e) KnGLL contours near the leading edge of all simulations.

over the flat plate surface. There is a good agreement between all CFD and the DSMC data in the range $x/L \geq 0.1$, while there is a large difference between all CFD simulation results and the DSMC data for $x/L \leq 0.1$. In order to explain this one, the local gradient length (GLL) Knudsen number is computed based on the density gradient of the gas flow in CFD as follows,

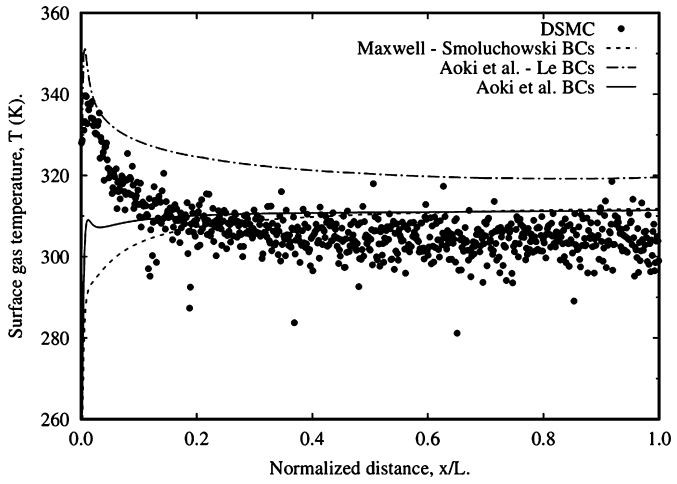

Fig. 6. Distribution of surface gas temperature over the flat plate.

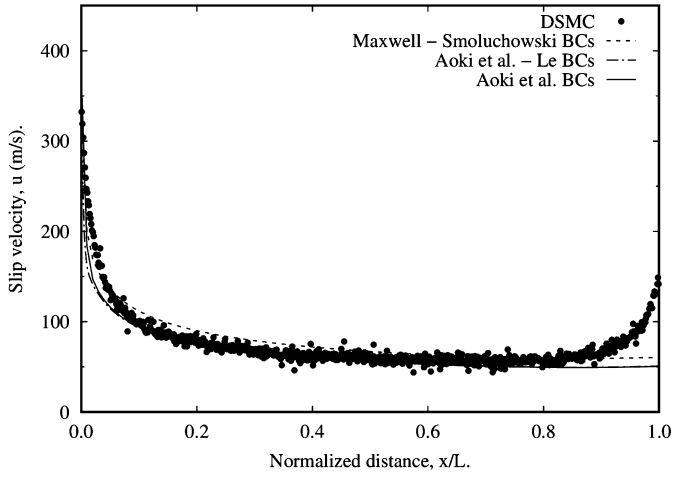

Fig. 7. Distribution of the slip velocity over the flat plate.

$$\mathrm{Kn}_{\mathrm{GLL}} = \lambda \frac{\|\nabla\rho\|}{\rho}, \tag{12}$$

where $\|\nabla\rho\|$ is magnitude of the density gradient. The $\mathrm{Kn}_{\mathrm{GLL}}$ is calculated in DSMC as follows,

$$\mathrm{Kn}_{\mathrm{GLL}} = \lambda_{\mathrm{DSMC}} \frac{\|\nabla\rho\|}{\rho}, \tag{13}$$

where the term λ_{DSMC} is computed as [20,21]

$$\lambda_{\mathrm{DSMC}} = \frac{2(5-2\omega)(7-2\omega)}{15}\sqrt{\frac{m}{2\pi k_B T}}\left(\frac{\mu_{\mathrm{DSMC}}}{\rho}\right),$$
$$\text{where } \mu_{\mathrm{DSMC}} = \mu_{\mathrm{ref}}\left(\frac{T}{T_{\mathrm{ref}}}\right)^{\omega}, \tag{14}$$

where subscript ref denotes the reference values, $T_{\mathrm{ref}} = 273$ K, ω is the macroscopic viscosity temperature exponent ($\omega = 0.5$ for the hard-sphere molecular model), and μ_{ref} is calculated as follows [20,21]:

$$\mu_{\mathrm{ref}} = \frac{15\sqrt{m\pi k_B T_{\mathrm{ref}}}}{2\pi d_{\mathrm{ref}}^2 (5-2\omega)(7-2\omega)}. \tag{15}$$

The values of $\mathrm{Kn}_{\mathrm{GLL}}$ over the flat plate surface are shown in Fig. 4. They obtain the peak values at the leading edge with the peak values of 1) 0.475 for simulation with the Maxwell–Smoluchowski conditions, 2) 0.55 for simulation with the Aoki et al. and Le conditions, 3) 0.48 for simulation with the Aoki et al. conditions, and 4) 0.57 for the DSMC data. It is noted that the continuum breakdown occurs whenever $\mathrm{Kn}_{\mathrm{GLL}} > 0.05$ [20,21]. Considering large $\mathrm{Kn}_{\mathrm{GLL}}$ value at the leading edge, the nonequilibrium effects are quite high there, and it is not expected that just improvement in slip and jump boundary conditions results in a suitable agreement between the CFD and Boltzmann solutions. In other words, the shear stress, which is described simply in conjunction with the *linear* constitutive relation of gradients of velocity, could not represent the true behavior of the gas viscous effects and boundary layer at highly non-equilibrium condition experienced at the leading edge. Thus, there should be a difference between the kinetic and continuum descriptions of the boundary layer in addition to the shock

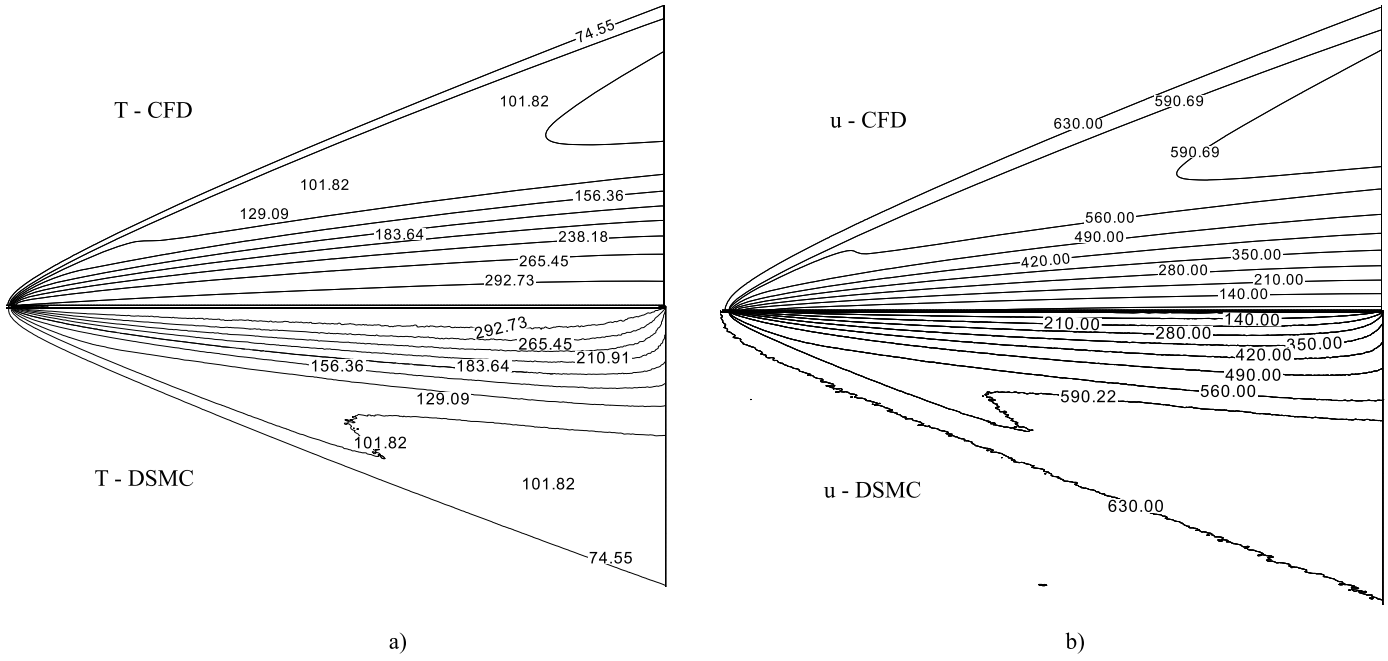

Fig. 8. Temperature and velocity magnitude contours over the flat plate case, a) temperature and b) velocity.

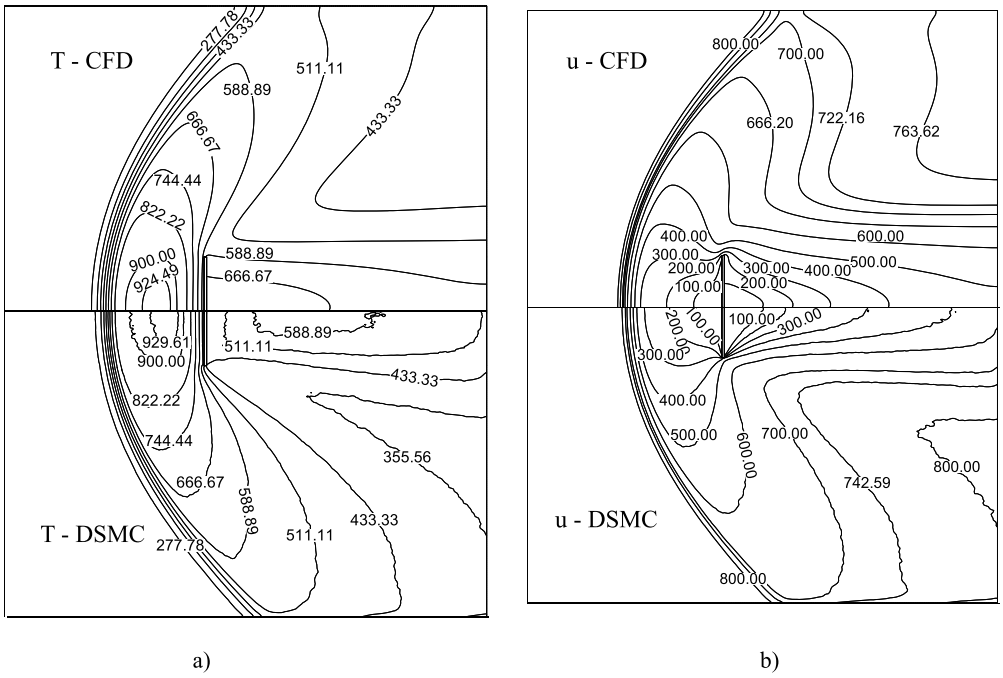

Fig. 9. Temperature and velocity magnitude contours for the vertical plate, a) temperature and b) velocity.

wave structure [21]. Boundary layer and shock thickness are different from the CFD and DSMC predictions. The DSMC prediction for shock is more diffusive than the CFD one, which is quite sharper. Moreover, from a mathematical view point, the model of inviscid gas near the leading edge is a singularity for differential operation. This is also true for viscous gas flows but the effect is weaker. This model differentiates the gas flow variations and that why there is a peak value there. The Boltzmann solution (DSMC) has an integral collision operator and integrates this singularity by the collision operator. In other words, it averages and smears in some sense the solution, this is the reason that DSMC shock wave is usually thicker than N–S–F solution. The KnGLL contours of CFD and DSMC simulations are found in Figs. 5a, 5b, 5c, and 5d to see how slip models change the shape of the shock at the leading edge. Magnitudes of Kn_{GLL} are higher at the shock wave and intersection of shock and boundary layer. There are the curved shocks at the leading edge, shown in Fig. 5e. The shock producing by the CFD simulation using the Aoki et al. and Le conditions is more curved than the two other CFD shocks and DSMC at the leading edge. This is expected by observing the peak values of the surface pressures at the leading edge that one using the Aoki et al. and Le conditions obtains the highest value.

Distribution of the CFD and DSMC surface gas temperatures is plotted in Fig. 6. The simulation results using the Le jump condition and the DSMC data obtain higher values near the leading edge while those using the Aoki et al. and Smoluchowski jump conditions obtain lower values. The formation of a shock, and the corresponding temperature jump across it occurs slightly downstream of the plate tip, yielding the results in Fig. 6 that temperature increases from the freestream temperature to a level downstream of the shock [22]. The results using the Le jump condition are close to the DSMC data at the leading edge. This may be explained by the significant effect of the viscous heat generation there. The simulation results of the Aoki et al. and the Smoluchowski jump conditions underpredict temperature near the leading edge, and generally give good agreement with the DSMC data over the flat plate for $x/L \geq 0.1$.

The slip velocities are presented in Fig. 7. All DSMC and CFD simulation results predict the peak values near the leading edge. They are 1) 344.2 m/s for simulation with the Maxwell–Smoluchowski conditions, 2) 317.23 m/s for simulation with the Aoki et al. and Le conditions, 3) 376.34 m/s for simulation with the Aoki et al. conditions, and 4) 332.36 m/s for the DSMC data. Thereafter, all of them gradually decrease in $x/L \leq 0.1$. In the range $0.1 \leq x/L \leq 1$, all CFD simulation results stay nearly constant over the flat plate while those of DSMC stay nearly constant until $x/L = 0.9$. All CFD simulation results generally agree with the DSMC data in $0.1 \leq x/L \leq 1$. The difference between the CFD and DSMC data for $x/L \geq 0.9$ may be affected by the flow separation near the trailing edge. The DSMC method can capture the flow separation while the CFD simulation results may not. Finally, Figs. 8a and 8b present the temperature and velocity magnitude contours for the CFD and DSMC simulations, respectively. The DSMC and CFD solutions perform differently in the boundary layer and shock wave regions. At the leading edge, a boundary layer is developed, and a curved shock is formed by the viscous effects, the compression across the shock, and the shock-boundary layer interaction.

4.2. *Vertical flat plate case, Kn = 0.07*

A bow shock is formed in front of the vertical flat plate, and is symmetrical with respect to the stagnation line depicted in Fig. 1b. A strong bow shock in front of the vertical plate is found in Fig. 9 that represents the temperature and velocity magnitude contours of the CFD and DSMC simulations. The shock stand-off distances predicted by both solutions are nearly the same. In the shock wave region, there is a high-temperature region and the velocity decreases due to the shock compression. There is a good agreement between the CFD and DSMC temperature contours in the front, and they are difference in the region behind the vertical plate. The surface quantities (p, T, $\mathbf{u}$) along the front surface of the vertical flat plate are presented in Figs. 10, 11 and 12 are symmetrical with respect to the stagnation line. Considering the surface gas pressure, there is a suitable agreement between all CFD simulation results and the DSMC data, as shown in Fig. 10. The Smoluchowski jump condition predicts higher temperatures than those using the Le and Aoki et al. jump conditions, presented in Fig. 11. The simulation re-

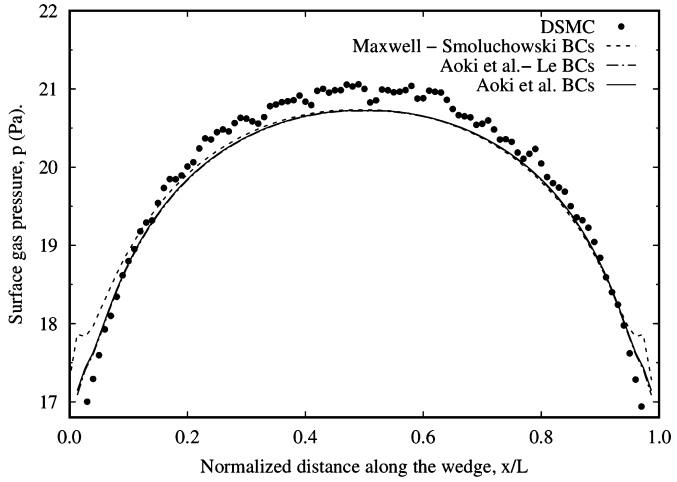

Fig. 10. Distribution of surface gas pressure along the vertical plate surface.

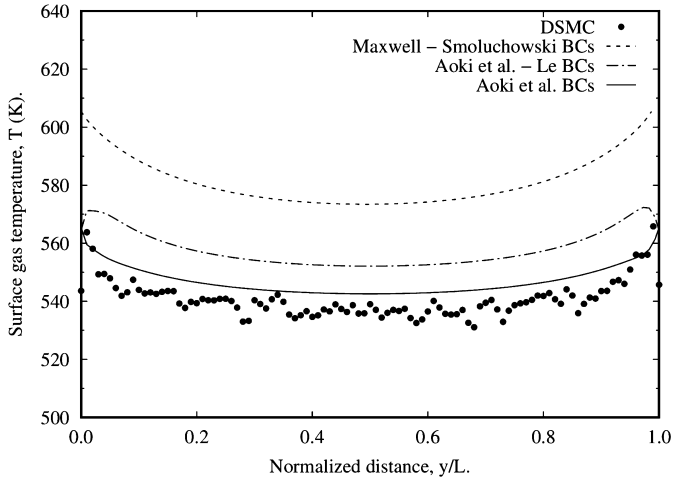

Fig. 11. Distribution of surface gas temperature along the vertical plate surface.

sults using the Aoki et al. jump condition are lowest, and close to the DSMC data.

The distribution of slip velocity along the front surface is shown in Fig. 12. The magnitudes of the slip velocity are largest at two boundaries of the plate ($y/L = 0$ and $y/L = 1$), and obtain the smallest value at the location $y/L = 0.5$. The slip velocities predicted by the Aoki et al. slip condition in two CFD simulations with the Aoki et al. – Le conditions and the Aoki et al. conditions are close together, and show a good agreement with the DSMC data.

4.3. Circular cylinder in cross-flow case, Kn = 0.01

The simulation results of the cylinder of the case Kn = 0.01 are presented in Figs. 13, 14, and 15. All CFD and DSMC simulations give the peak pressure at the stagnation point ($\Phi = 0$-deg.) which are close together. Past the stagnation point, the surface pressure is gradually reduced along the cylinder surface from $\Phi = 0$-deg. to $\Phi = 90$-deg. There is good agreement between all CFD simulations and DSMC data, seen in Fig. 13.

Fig. 14 presents the surface gas temperatures along the cylinder surface. The Smoluchowski jump boundary condition overpredicts the temperature along the cylinder surface. The temperatures using the Aoki et al. and the Le jump conditions are close together in 0-deg. $\leq \Phi \leq$ 40-deg. The Le jump condition predicts higher temperatures than the Aoki et al. jump condition in 40-deg. $\leq \Phi \leq$ 90-deg. This may be explained that the viscosity in the Le jump condition is calculated at the gas temperature near the surface

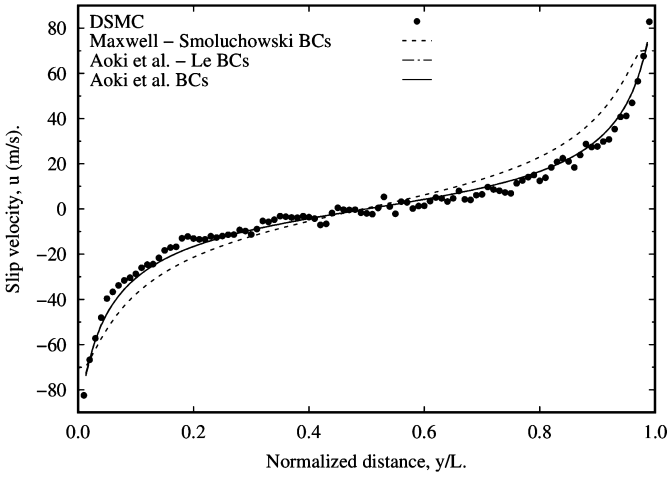

Fig. 12. Distribution of slip velocity along the vertical plate surface.

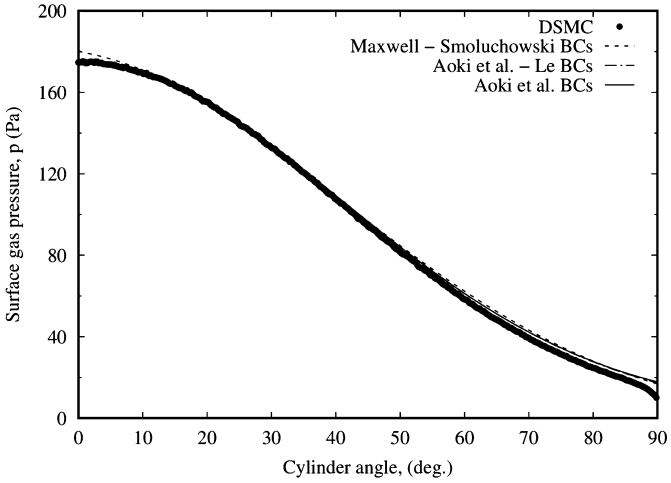

Fig. 13. Distribution of surface gas pressure along the cylinder surface, Kn = 0.01.

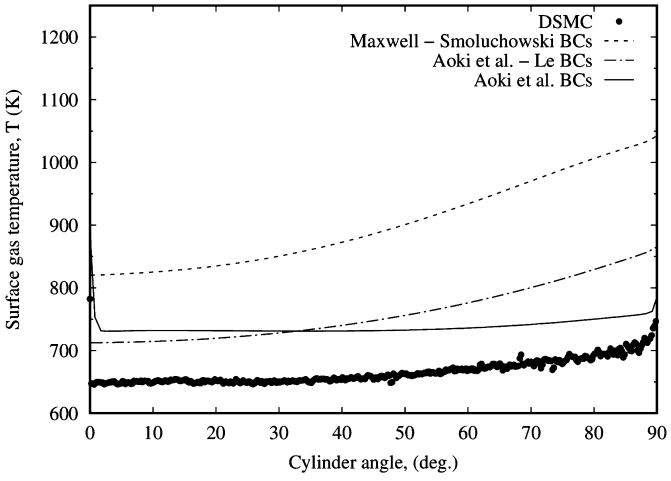

Fig. 14. Distribution of surface gas temperature along the cylinder surface, Kn = 0.01.

while that is computed at the wall temperature in the Aoki et al. jump condition. This leads to the viscosity in the Le jump condition to be higher than that in the Aoki et al. jump condition. In overall, the temperature using the Aoki et al. jump condition is close to the DSMC data while that of the Le jump condition is not. The average errors between them and the DSMC data are 14.33%

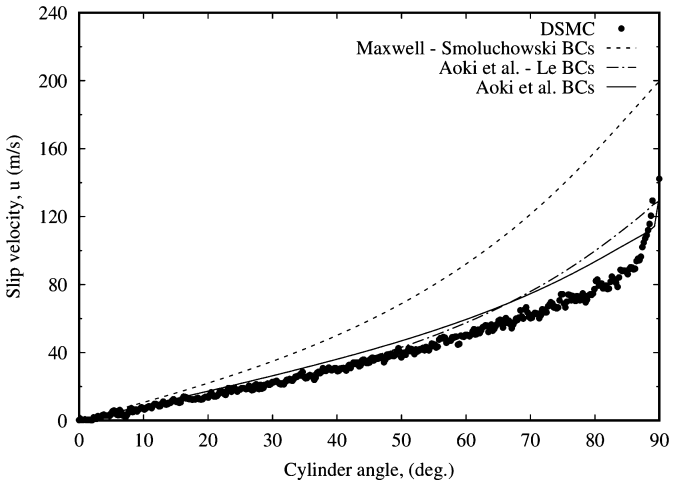

Fig. 15. Distribution of slip velocity along the cylinder surface, Kn = 0.01.

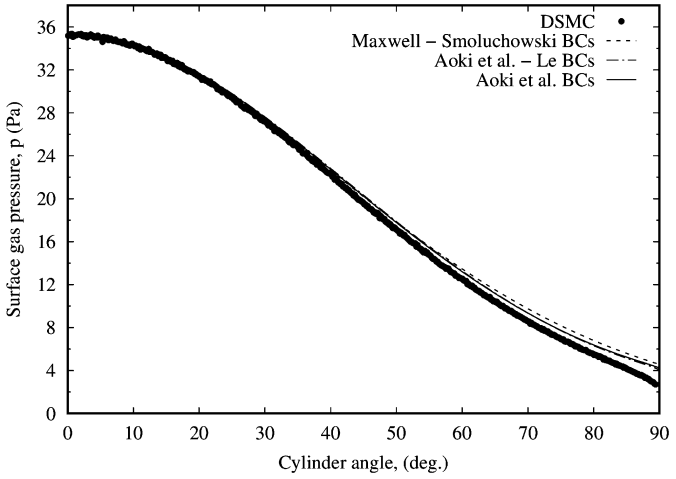

Fig. 16. Distribution of surface gas pressure along the cylinder surface, Kn = 0.05.

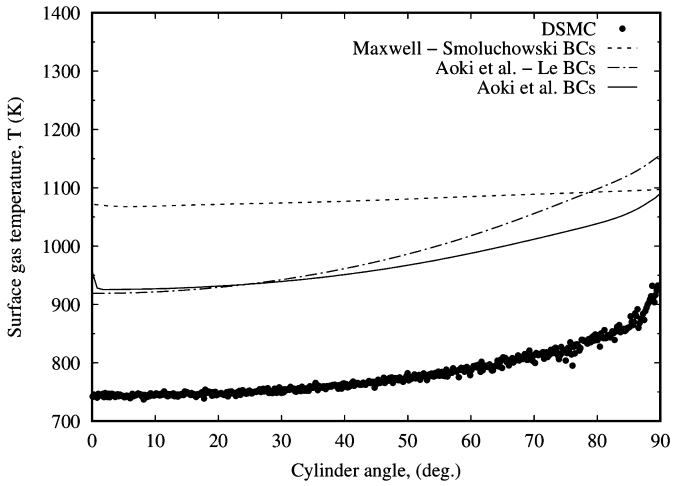

Fig. 17. Distribution of surface gas temperature along the cylinder surface, Kn = 0.05.

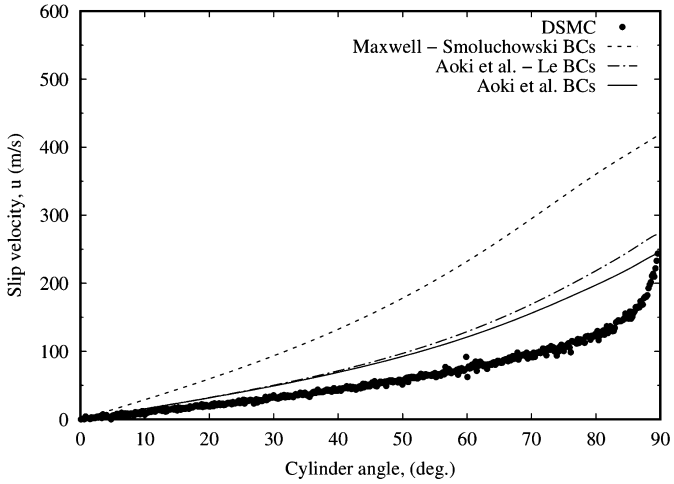

Fig. 18. Distribution of slip velocity along the cylinder surface, Kn = 0.05.

for the simulation with the Le jump condition, and 10.7% for the simulation with the Aoki et al. jump condition.

Slip velocities along the cylinder surface are shown in Fig. 15. At the stagnation point, they are approximate the value of zero. Thereafter, they gradually increase along the surface cylinder from $\Phi = 0$-deg. to $\Phi = 90$-deg., and obtain the peak values at the location $\Phi = 90$-deg. The Maxwell slip boundary condition predicts higher slip velocities than the Aoki et al. slip condition. The slip velocities using the Aoki et al. slip condition in two CFD simulations with the Aoki et al. – Le conditions and Aoki et al. conditions are close to the DSMC data, and their average errors in comparing the DSMC data are 13.33% and 15.13%, respectively.

4.4. Circular cylinder in cross-flow case, Kn = 0.05

Considering the surface gas pressure in Fig. 16, all CFD simulation results give suitable agreement with the DSMC data. They obtain the peak values at the stagnation point ($\Phi = 0$-deg.), and thereafter they gradually decrease along the cylinder surface. The surface gas temperatures are presented in Fig. 17. All CFD and DSMC simulation results obtain the lowest value at the stagnation point, and then increase along the cylinder surface. All CFD jump conditions overpredict the temperatures along the cylinder surface. The temperatures using the Le and Aoki et al. jump conditions are close together in 0-deg. $\leq \Phi \leq$ 45-deg. The temperatures using the Aoki et al. jump condition are lower than those given by the Le jump condition in 45-deg. $\leq \Phi \leq$ 90-deg. This may be explained that 1) the viscosity calculating at the wall temperature in the Aoki et al. is lower than that computing at the gas temperature near the surface in the Le jump condition, and 2) the slip velocities predicted by the simulation with the Aoki et al. and Le conditions are higher than those given by the simulation with Aoki et al. conditions in 45-deg. $\leq \Phi \leq$ 90-deg. In overall, temperatures using the Aoki et al. jump condition give relatively good agreement with the DSMC data along the cylinder surface.

Fig. 18 presents the distribution of the slip velocity along the cylinder surface. All CFD and DSMC simulation results obtain approximately the value of zero at the stagnation point, and then they gradually increase along the cylinder surface. The slip velocity using the Aoki et al. slip condition is close to the DSMC data while those using the Maxwell slip solution is not.

For the completeness of the circular cylinder case, the temperature and velocity magnitude contours predicted by both CFD and DSMC are found in Figs. 19 and 20 for the Kn = 0.01 and Kn = 0.05 cases, respectively. The temperature contours represent the typical flow features found in a blunt body flow as a fairly shockwave standing off from the body, and a high temperature region following the shock. The translational energy is converted into thermal energy with the decrease in velocity due to shock compression. A thermal boundary layer that gradually thickens around the cylinder [20]. Overall agreement between CFD and DSMC temperature contours is generally good for both of cases, with some small differences in the shock structure, shown in Figs. 19a and

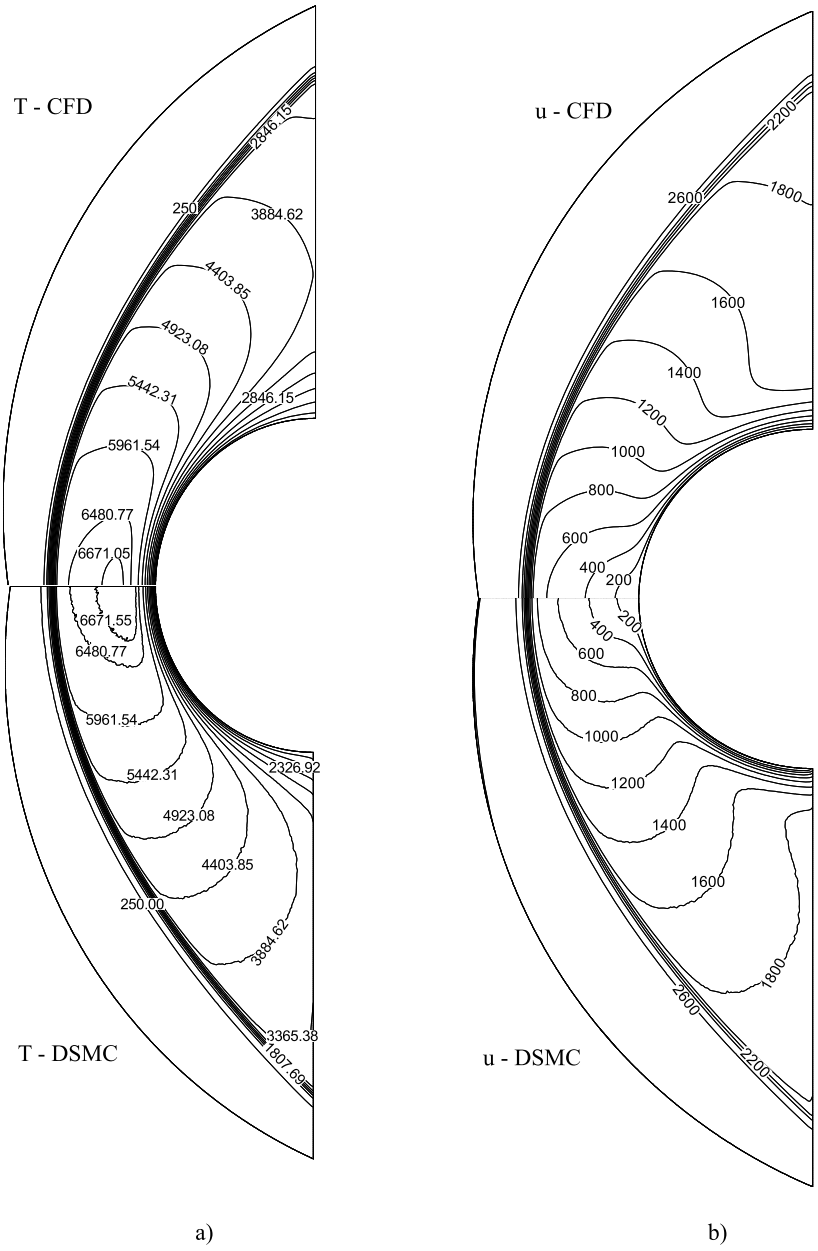

Fig. 19. Temperature and velocity magnitude contours of the cylinder, Kn = 0.01, a) temperature and b) velocity.

20a. The velocity magnitude contours of CFD and DSMC solutions give good agreement for the case Kn = 0.01, seen in Fig. 19b, but there is the small difference between those for the case Kn = 0.05, seen in Fig. 20b. The shock stand-off distance predicted by both methods is nearly the same as is the thermal boundary layer thickness at the stagnation point for both of cases [20]. When Kn increases the shock stand-off distance also increases.

4.5. Wedge case, Kn = 0.05

The results of the surface quantities (p, T, $\mathbf{u}$) are plotted as a function of the distance, S, along the wedge surface normalized by the length L. Similar to the distribution of the surface pressure of the flat plate case, Fig. 21 shows that the surface gas pressures are highest near the leading-edge with the peak values of 1) 24.1 Pa for the simulation with the Maxwell–Smoluchowski conditions, 2) 24 Pa for the simulation with the Aoki et al. – Le conditions, 3) 23.25 Pa for the simulation with the Aoki et al. conditions, and 4) 16.5 Pa for the DSMC data. Thereafter, they gradually decrease along the wedge surface. The simulation with the Maxwell–Smoluchowski conditions overpredicts the surface gas pressure along the wedge surface. The results of the simulation with the Aoki et al. conditions are close to the DSMC data for $S/L \geq 0.2$.

Fig. 22 shows the distribution of the surface gas temperature. They obtain the peak values near the leading-edge with the values of 1) 2764 K for the Smoluchowski jump condition, 2) 2331 K for the Le jump condition, 3) 2587 K for the Aoki et al. jump condition, and 4) 2578 K for the DSMC data. Past the leading-edge, the gas temperatures gradually decrease along the wedge surface. The Smoluchowski condition overpredicts the surface gas temperature along the wedge surface. The Le and Aoki et al. jump conditions include the terms of velocity and gradient of the velocity of gas flows. The slip velocity in simulation with the Aoki et al. – Le condition is lower than that given by the simulation with the Aoki et al. conditions, seen in Fig. 23. This may result in the temperatures using the Le jump condition are lower than those using the Aoki

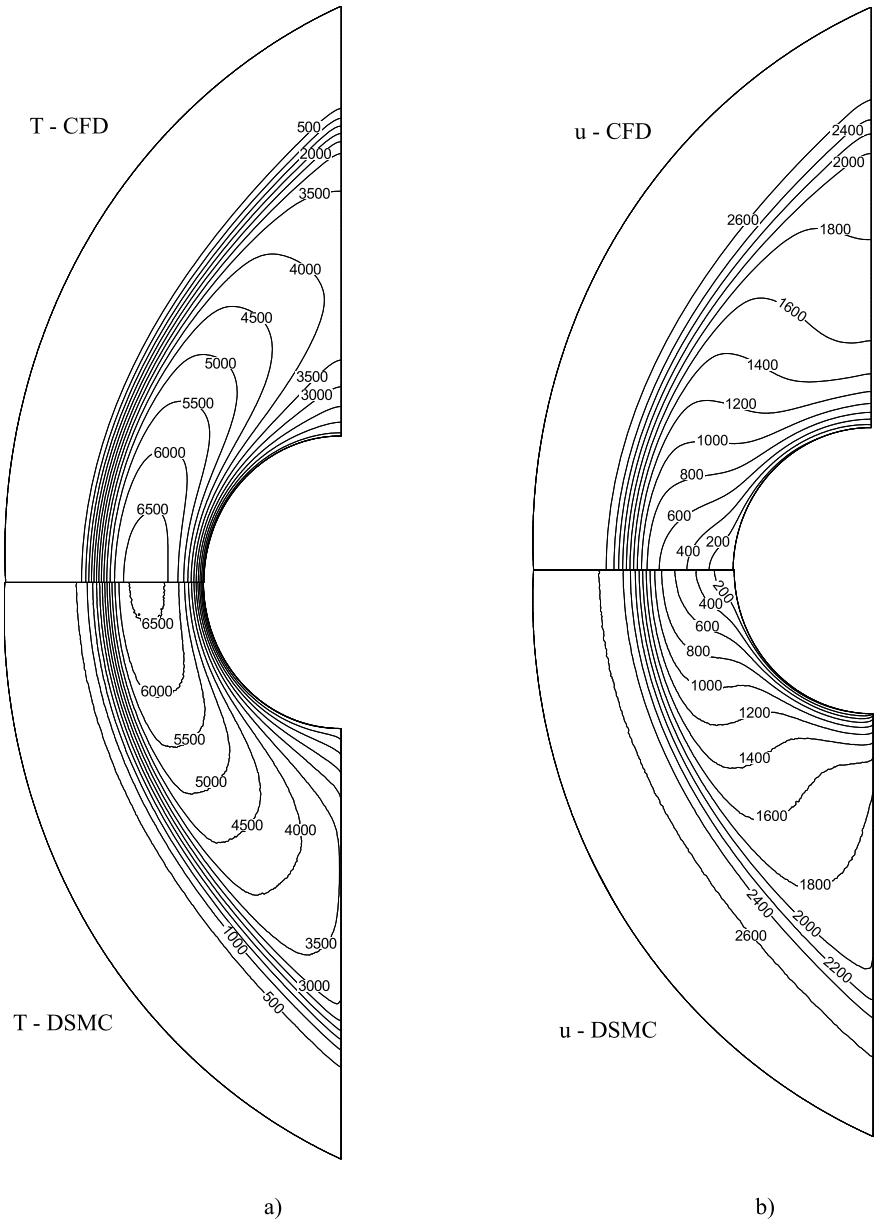

Fig. 20. Temperature and velocity magnitude contours of the cylinder, Kn = 0.05, a) temperature and b) velocity.

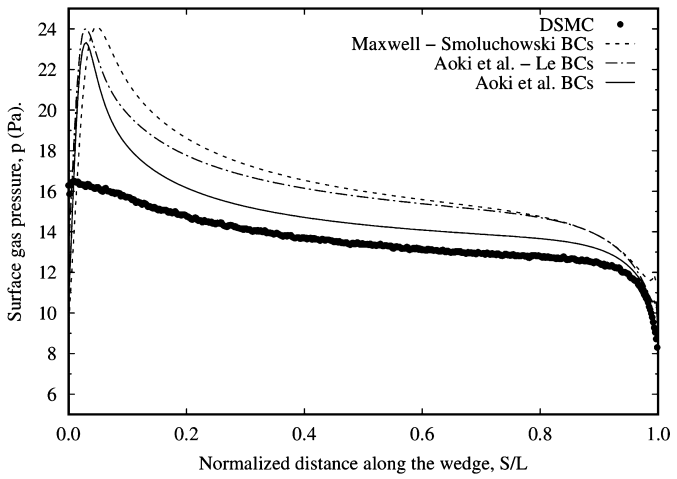

Fig. 21. Distribution of surface gas pressure along the wedge surface.

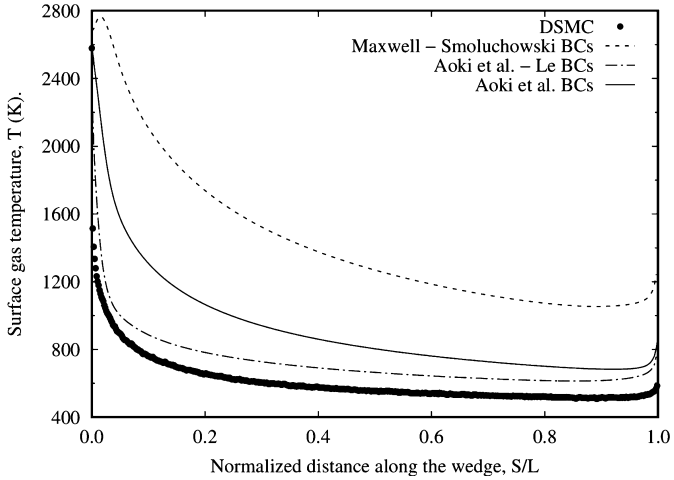

Fig. 22. Distribution of surface gas temperature along the wedge surface.

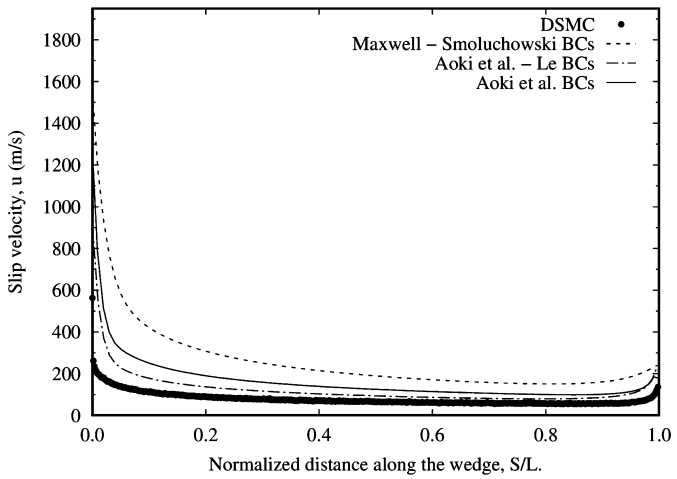

Fig. 23. Distribution of slip velocity along the wedge surface.

et al. jump condition, and give good agreement with the DSMC data along the wedge surface. Temperatures using the Aoki et al. jump condition do not give good agreement with the DSMC data.

It is similar to the distribution of the surface gas temperature. At the leading edge the slip velocities obtain the peak values of 1) 1543.75 m/s for the simulation with the Maxwell–Smoluchowski conditions, 2) 908.95 m/s for the simulation with the Aoki et al. – Le conditions, 3) 1263.22 m/s for the simulation with the Aoki et al. conditions, and 4) 563.79 m/s for the DSMC data, seen in Fig. 23. Past the leading edge, the slip velocities quickly decrease to a nearly constant finite value until the location $S/L = 1$. The results using the Maxwell slip condition obtain higher slip velocity than those given by the Aoki et al. slip condition. The slip velocities of the simulation with the Aoki et al. – Le conditions are close to the DSMC data. The effect of the Le and the Aoki et al. jump conditions may result in the difference of the slip velocities using the Aoki et al. slip solution in $0 \leq S/L \leq 0.25$. The CFD and DSMC temperature and velocity magnitude contours of the wedge case are shown in Fig. 24. There is a high temperature region near

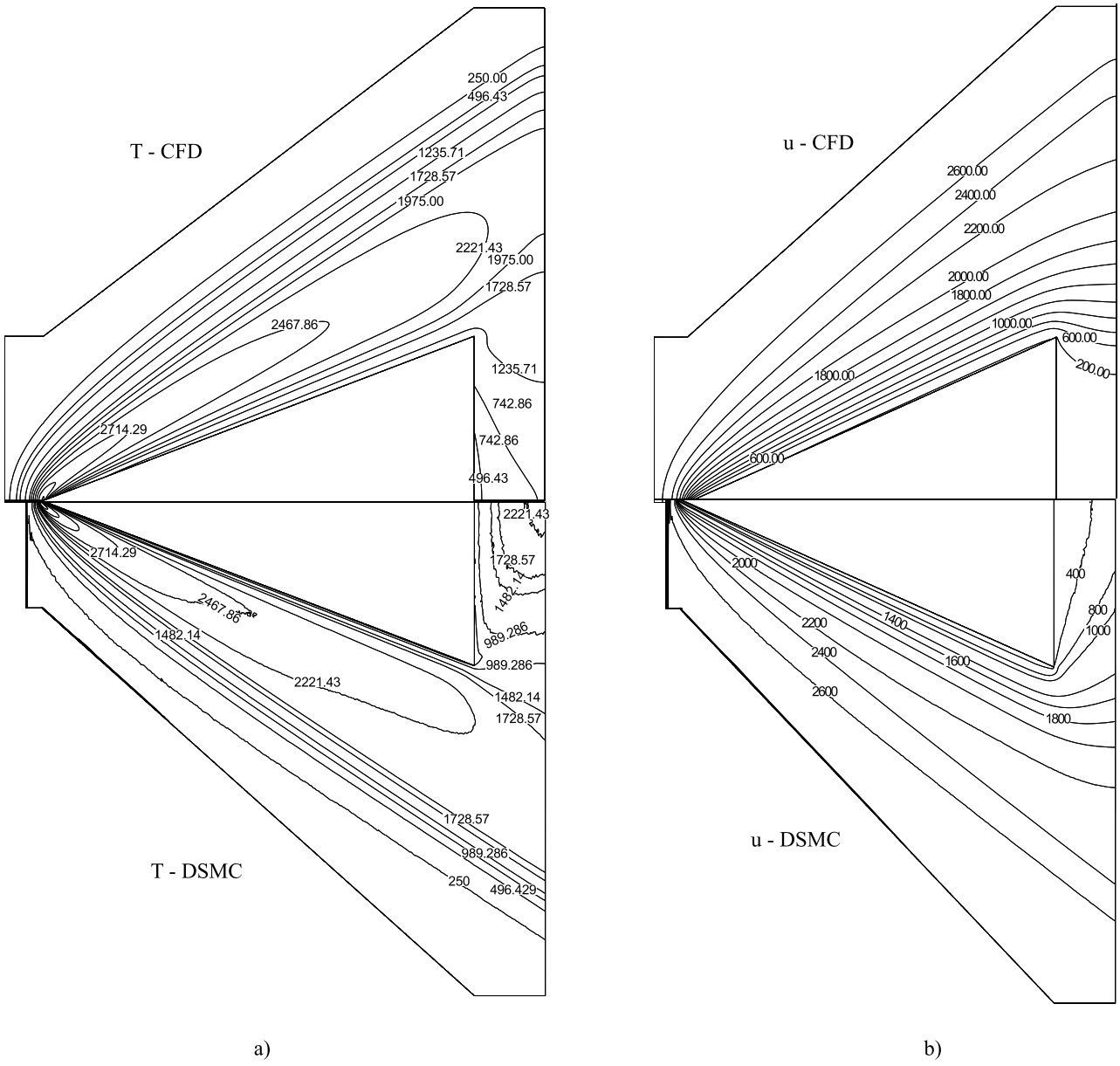

Fig. 24. Temperature and velocity magnitude contours of the wedge case, a) temperature and b) velocity.

the leading edge. The temperature and velocity magnitude contours seem to agree in the majority of the computational domain, but there are differences in the wake region. Similar to the flat plate case, there is a curved shock at the leading edge, and the flow is compressed through this shock. It forms a small distance in front of the wedge.

5. Discussions

The DSMC data of slip velocity are generally lowest in most cases considering in the present work. This leads to the DSMC surface gas temperatures are also lowest because they are calculated from the components of the peculiar velocity in equation (11). In all cases, the Aoki et al. slip and jump conditions generally predict a lower temperature and slip velocity than other slip and jump conditions, except the surface gas temperatures of the wedge case. The simulation results using the Aoki et al. slip and jump conditions are close to the DSMC data. This may be explained: 1) the viscosity and thermal conductivity are calculated at the wall temperature (T_w) while those in the Maxwell, Smoluchowski and Le conditions are computed at the gas temperature near the surface. The viscosity and thermal conductivity are proportional to the temperature, and the surface gas temperatures obtained in the present work are always greater than the wall temperature in high-speed rarefied gas simulations, and 2) the Aoki et al. slip and jump conditions were derived based on the Boltzmann equations with the first-order Chapman–Enskog solution, and the analysis of the Knudsen layer.

6. Conclusion

In this paper we have evaluated the Aoki et al. slip and jump boundary conditions for high-speed rarefied gas flows that they were mathematically derived based on the Boltzmann equation. The simulation results using the Aoki et al. slip and jump conditions have given good agreement with the DSMC data for the sharp-leading-edge and blunt surfaces, and are better than those of the conventional Maxwell, Smoluchowski, and Le boundary conditions. The simulation results obtained suggest that the Aoki et al. slip and jump conditions are an alternative choice for the surface nonequilibrium boundary conditions in CFD simulation for high-speed rarefied gas flow that solves the N–S–F equations.

Declaration of Competing Interest

None of competing interest.

Acknowledgements

N.T.P.L and T.N.T would like to thank the NAFOSTED. This research is funded by Vietnam National Foundation for Science and Technology Development (NAFOSTED) under grant number 107.03-2018.27.

References

[1] J.C. Maxwell, On stresses in rarefied gases arising from inequalities of temperature, Philos. Trans. R. Soc. 170 (1879) 231–256.
[2] M. von Smoluchowski, Über Wärmeleitung in verdünnten Gasen, Ann. Phys. Chem. 64 (1898) 101–130.
[3] N.T.P. Le, C. White, J.M. Reese, R.S. Myong, Langmuir–Maxwell and Langmuir–Smoluchowski boundary conditions for thermal gas flow simulations in hypersonic aerodynamics, Int. J. Heat Mass Transf. 55 (2012) 5032–5043.
[4] T. Gökçen, R.W. MacCormack, Nonequilibrium Effects for Hypersonic Transitional Flows Using Continuum Approach, AIAA paper, No. 1989–0461, 1989.
[5] R.S. Myong, Gaseous slip model based on the Langmuir adsorption isotherm, Phys. Fluids 16 (2004) 104–117.
[6] S. Shen, G. Chen, R.M. Crone, M. Anaya-Dufresne, A kinetic theory based first order slip boundary condition for gas flow, Phys. Fluids 19 (2017) 086101.
[7] N.T.P. Le, E. Roohi, A new form of the second order temperature jump boundary condition in the low speed nano/microscale and hypersonic rarefied gas flow simulations, Int. J. Therm. Sci. 89 (2015) 51–59.
[8] N.T.P. Le, A. Shoja Sani, E. Roohi, Rarefied gas flow simulations of NACA 0012 airfoil and sharp 25-55 biconic subject to high order nonequilibrium boundary conditions in CFD, Aerosp. Sci. Technol. 41 (2015) 274–288.
[9] M. Mahdavi, N.T.P. Le, E. Roohi, C. White, Thermal rarefied gas flow investigations through micro/nano backward-facing step: comparison of DSMC and CFD subject to hybrid slip and jump boundary conditions, Numer. Heat Transf., Part A, Appl. 66 (2014) 733–755.
[10] K. Aoki, C. Baranger, M. Hattori, S. Kosuge, G. Martalo, J. Mathiaud, L. Mieussens, Slip boundary conditions for the compressible Navier–Stokes equations, J. Stat. Phys. 169 (2017) 744–781.
[11] M. Hattori, S. Kosuge, K. Aoki, Slip boundary conditions for the compressible Navier–Stokes equations for a polyatomic gas, Phys. Rev. Fluids 3 (2018) 063401.
[12] K. Aoki, R. Kagaya, S. Kosuge, H. Yoshida, Numerical analysis of the Taylor-Vortex flow of a slightly rarefied gas, in: The AIP Conference Proceedings of the 29th International Symposium on Rarefied Gas Dynamic, vol. 1628, 2014, pp. 60–67.
[13] N.T.P. Le, N.A. Vu, L.T. Loc, New type of Smoluchowski temperature jump condition considering the viscous heat generation, AIAA J. 55 (2017) 474–483.
[14] N.T.P. Le, N.H. Tran, T.N. Tran, Modified Patterson temperature jump condition considering viscous heat generation, Int. J. Heat Mass Transf. 126 (2018) 1267–1274.
[15] E.H. Kennard, Kinetic Theory of Gases, McGraw-Hill, New York, 1938.
[16] S.H. Maslen, On heat transfer in slip flow, J. Aerosp. Sci. 25 (1958) 400–401.
[17] OpenFOAM, http://www.openfoam.org, 11/2018.
[18] E. Roohi, S. Stefanov, Collision partner selection schemes in DSMC: from micro/nano flows to hypersonic flows, Phys. Rep. 656 (2016) 1–38.
[19] G.A. Bird, The DSMC Method, Clarendon, Oxford, 2013.
[20] A. Lofthouse, L.C. Scalabrin, I.D. Boyd, Velocity slip and temperature jump in hypersonic aerothermodynamics, J. Thermophys. Heat Transf. 22 (2008) 38–49.
[21] M. Darbandi, E. Roohi, A hybrid DSMC/Navier–Stokes frame to solve mixed rarefied/nonrarefied hypersonic flows over nano-plate and micro-cylinder, Int. J. Numer. Methods Fluids 72 (2013) 937–966.
[22] C.J. Greenshields, J.M. Reese, Rarefied hypersonic flow simulations using the Navier–Stokes equations with non-equilibrium boundary conditions, Prog. Aerosp. Sci. 52 (2012) 80–87.